

Suzaku X-ray spectral study of the Compton-thick Seyfert galaxy NGC 5135

Veeresh Singh^{1,2*}, Guido Risaliti^{3,4}, Valentina Braito⁵ and Prajval Shastri¹

¹Indian Institute of Astrophysics, Bangalore 560034, India

²Department of Physics, University of Calicut, Calicut 673635, India

³INAF-Osservatorio di Arcetri, Largo E. Fermi 5, I-50125 Firenze, Italy

⁴Harvard-Smithsonian Center for Astrophysics, 60 Garden St. Cambridge, MA 02138, USA

⁵Department of Physics and Astronomy, University of Leicester, University Road, Leicester LE1 7RH, UK

Accepted xxxx xxxxxx xx; Received xxxx xxxxxx xx; in original form xxxx xxxxxx xx

ABSTRACT

We present the 0.5 - 50 keV *Suzaku* broad-band X-ray spectral study of the Compton-thick AGN in NGC 5135. The *Suzaku* observation provides the first detection of NGC 5135 above 10 keV that allowed us, for the first time, to estimate the absorbing column density, the intrinsic X-ray luminosity, the strength of the reflection component and the viewing angle of the torus for this AGN. The 0.5 - 10 keV spectrum of NGC 5135 is characterized by the standard components for a Compton-thick source: a scattered continuum, a prominent Fe K α emission line (EW \sim 2.1 keV) and a soft excess. At higher energies ($E > 10$ keV) the intrinsic AGN continuum shows up, implying an absorbing column density of the order of $\sim 2.5 \times 10^{24}$ cm $^{-2}$ and the intrinsic 2.0 - 10 keV X-ray luminosity of $\sim 1.8 \times 10^{43}$ erg s $^{-1}$. Assuming a toroidal geometry of the reprocessing material we show that an edge-on view of the obscuring torus is preferred in this source.

Key words: galaxies: active, galaxies: individual: NGC 5135, X-rays: galaxies

1 INTRODUCTION

Seyfert galaxies host active galactic nuclei (AGN) powered by accretion on to supermassive black hole. The luminous accreting engine is supposedly surrounded by obscuring material having a torus-like geometry (Antonucci 1993). When the obscuring torus intercepts the observer's line-of-sight (*i.e.*, type 2 AGN), the absorbing column density (N_{H}) for X-ray photons originating from AGN is typically higher than 10^{22} cm $^{-2}$ (Cappi et al. 2006). In mildly Compton-thick AGN ($N_{\text{H}} \sim$ a few times of 10^{24} cm $^{-2}$), the primary emission is strongly suppressed below 10 keV and is seen only above 10 keV, while in heavily Compton-thick AGN ($N_{\text{H}} \geq 10^{25}$ cm $^{-2}$) the primary emission is strongly depressed even at energies above 10 keV due to Compton down-scattering (Matt et al. 2000). In *Chandra*, *XMM-Newton* and earlier observations sensitive only up to 10 keV, Compton-thick AGNs have been identified only by using diagnostic properties such as high equivalent width (EW) of Fe K α line (≥ 1.0 keV, Bassani et al. (1999)), low flux ratio of hard X-ray (2.0 - 10.0 keV) to [OIII] $\lambda 5007\text{\AA}$ line emission (Maiolino et al. 1998) and there are no measurements of the true value of the absorbing col-

umn density. There is evidence that obscured AGNs are much more numerous than unobscured AGNs, both in the local universe and at intermediate to high redshifts (Risaliti et al. 1999; Hasinger 2008). In recent years, observations from INTEGRAL, *Swift*, and *Suzaku* have increased the number of Compton-thick sources detected in hard X-ray (Della Ceca et al. 2008; Beckmann et al. 2009; Tueller et al. 2008; Severgnini et al. 2011). However, the number of Compton-thick sources whose broad-band spectra are analyzed in detail is still limited. In this paper we present the *Suzaku* broad-band X-ray spectral properties of NGC 5135, which is one of the brightest known Compton-thick Seyfert type 2 galaxies, with no previous X-ray observations above 10 keV. NGC 5135 has not been detected above 10 keV by any of the hard X-ray detectors, *e.g.*, *BeppoSAX*-PDS, *Swift*-BAT, *INTEGRAL*-IBIS, other than *Suzaku* HXD-PIN. NGC 5135 is a relatively nearby (redshift $z \simeq 0.014$) galaxy and optically classified as a Seyfert type 2 on the basis of emission line ratios (Phillips et al. 1983). IR and UV studies have shown that NGC 5135 also contains a powerful compact nuclear starburst (Bedregal et al. 2009; González Delgado et al. 1998). The higher spatial resolution of *Chandra* ($\sim 0.5''$) enables isolation of the AGN and starburst emissions, and has shown that the AGN in NGC 5135 is completely obscured by a col-

* E-mail: veeresh@iiap.res.in

umn density $N_{\text{H}} \geq 10^{24} \text{ cm}^{-2}$ (Levenson et al. 2004). The Compton-thick obscuration around AGN in NGC 5135 is also inferred from ASCA observations (Turner et al. 1997). Fukazawa et al. (2011) used the *Suzaku* data and report the presence of high absorbing column density ($N_{\text{H}} \sim 2.0 \times 10^{24} \text{ cm}^{-2}$) and a strong (EW $\sim 1.6 \text{ keV}$) Fe K α emission line in NGC 5135. The primary aim of Fukazawa et al. (2011) is to study the properties of the Fe K line features and its correlation with the absorbing column density and AGN luminosity for a sample of Seyfert galaxies. In this paper, we discuss the detailed broad-band X-ray spectral analysis of NGC 5135 using the same *Suzaku* data, with the aim to characterize the reprocessing material around the AGN.

2 OBSERVATIONS AND DATA REDUCTION

Suzaku observed NGC 5135 on 2007 July 03 (observation ID 702005010) with an exposure time of $\sim 52.5 \text{ ks}$. *Suzaku* (Mitsuda et al. 2007) carries four X-ray telescopes (XRTs: Serlemitsos et al. (2007)) with X-ray CCD cameras (XIS) at their focal-planes. The XISs are sensitive to 0.2 - 12.0 keV energy band with $18' \times 18'$ field-of-view. Among the four XIS CCDs, three (XIS 0, 2, and 3) are front-illuminated (FI) and one (XIS1) is back-illuminated (BI) (Koyama et al. 2007). There are no observations with XIS2, due to a malfunction in November 2006. *Suzaku* also has a non-imaging hard X-ray detector (HXD: Takahashi et al. (2007)) which has two types of detectors, the PIN and the GSO, which are sensitive in 10 - 700 keV energy band.

NGC 5135 was detected by XIS 0, 1, 3 and HXD-PIN. We obtained the XIS and HXD event files and reduced these by following the standard procedure described in the *Suzaku* reduction guide¹, and using the most recent calibration files. For the low-energy instruments (XISs), the source spectra were extracted from a circular region of $2.4'$ radius centered on the source. The background spectra were extracted from two circular regions of $2.2'$ radius offset from the source and calibration sources. The XIS response (rmfs) and ancillary response (arfs) files were produced with the ftools tasks *xisrmfgen* and *xissarmfgen*, respectively, and the latest calibration files were used. The spectra of the two front-illuminated CCDs (XIS0 and XIS3) were merged. The net XIS source spectra were binned to have minimum signal-to-noise ratio (S/N) of 4 in each energy bin and χ^2 statistics has been used. For the HXD-PIN, we used the rev2 data that include all 4 cluster units and the best available background (Fukazawa et al. 2009), which accounts for the instrumental background (NXB, Takahashi et al. (2007)) with systematic uncertainties of $\sim 1.3\%$ (at 1σ). We then simulated a spectrum for the cosmic X-ray background counts and added it to the instrumental one. Using this background NGC 5135 is detected in the 13 - 50 keV band at $\sim 7\%$ above the background with a net count rate of $(2.7 \pm 0.2) \times 10^{-2} \text{ cts s}^{-1}$ (a total of ~ 1400 net source counts have been collected), corresponding to a signal-to-noise ratio (S/N) ~ 9.2 . Since the HXD-PIN is a non-imaging detector and has large field-of-view ($\sim 0.56 \text{ deg} \times 0.56 \text{ deg}$), we checked that the HXD-PIN detection of NGC 5135 is not caused and/or contaminated

by any other source. In order to do this, we searched the HEASARC/NED database for the potential hard X-ray ($E > 10 \text{ keV}$) emitting sources in a circular region of the radius of $17'$ around the NGC 5135. The *Swift*, *INTEGRAL* and *BeppoSAX* catalogs do not report any hard X-ray source detection in this area. The *Chandra*, *ASCA* master catalogs report only NGC 5135 as the potential hard X-ray emitting source. During the *Suzaku* observations, NGC 5135 was placed at the HXD nominal pointing, therefore, in the spectral analysis, we used a cross-calibration constant of 1.18 between the HXD and XIS spectra, as suggested by the *Suzaku*-HXD calibration team.

3 SUZAKU X-RAY SPECTRAL FIT

The 2.0 - 10 keV *Suzaku* data can be fitted with a flat power law ($\Gamma \sim 1.4$) and a Gaussian for Fe K α line of high EW ($\sim 3.0 \text{ keV}$), which is broadly similar to the fit reported by previous *Chandra* observation (Levenson et al. 2004). The flat power law and high EW of Fe K α line are indicative of the heavily obscured AGN. In order to characterize the X-ray emission from heavily absorbed AGN, we attempt to fit the 0.5 - 50 keV *Suzaku* data using physically motivated models. In order to avoid the complexity of the soft component ($E < 2.0 \text{ keV}$) we first attempted to fit the 2.0 - 50 keV spectrum with a basic model of obscured AGN *i.e.*, an absorbed power law representing the AGN X-ray emission transmitted through a cold absorber and an unabsorbed power law for the scattered component. This simple model gives $\chi^2/\text{d.o.f.} \sim 182/31$ and leaves large residuals around 6.4 keV with an emission line-like shape. Adding a Gaussian profile for the Fe K α at 6.4 keV improves the fit very significantly and gives the fit statistics $\chi^2/\text{d.o.f.} \sim 39/29$, with $N_{\text{H}} \sim 2.5 \times 10^{24} \text{ cm}^{-2}$, $\Gamma \sim 1.8$ for the absorbed component, a steep power law ($\Gamma \sim 2.7$) accounting for the emission below 10 keV and the equivalent width (EW) of Fe K α line $\sim 2.1 \text{ keV}$. The Fe K α line is fitted with a narrow Gaussian (σ fixed to 10 eV) and any increase in the line width worsen the fit. There are no signatures for the Fe K β or the ionized component of Fe K α line emission in the residuals and the addition of any Gaussian component for such lines worsen the fit statistics. If the photon index (Γ) of the unabsorbed power law component is fixed to the value equal to the photon index of the absorbed power law component, the fit statistics does not improve and this fit results $\Gamma \sim 2.1$ with little increase in the column density ($N_{\text{H}} \sim 2.6 \times 10^{24} \text{ cm}^{-2}$), while the other parameters remain nearly unchanged. Considering the high N_{H} of the absorbed component and the high EW of the Fe K α line as the indicative of the presence of reflection component, we added the PEXRAV (Magdziarz & Zdziarski 1995) model component which represents the emission reflected from a neutral medium. The addition of reflection component gives $\chi^2/\text{d.o.f.} \sim 33/28$ (model 'M1' in Table 1) *i.e.*, improvement of $\Delta\chi^2 \sim 6$ for 1 d.o.f. at the significance level of 90%. The photon index of the reflected component (PEXRAV) was fixed equal to the transmitted component and the reflection scaling factor was fixed to -1, while all other parameters of the PEXRAV model were kept to their default values. We note that an equally good fit is obtained if we fix the photon-index of the intrinsic power law to 1.9, the canonical value for Seyferts (Nandra & Pounds 1994). How-

¹ <http://heasarc.gsfc.nasa.gov/docs/suzaku/analysis/abc/>

ever, as expected, a higher value of the absorbing column density ($N_{\text{H}} \sim 2.9 \times 10^{24} \text{ cm}^{-2}$) is required to account for the steeper power law. In order to assess the importance of the reflection component, we estimated the 2.0 - 10 keV X-ray fluxes associated with the unabsorbed power law and the **PEXRAV** (reflection) model components using the model ‘M1’. The 2.0 - 10 keV X-ray fluxes associated with the unabsorbed power law and the **PEXRAV** (reflection) model components are $\sim 1.27 \times 10^{-13} \text{ erg cm}^{-2} \text{ s}^{-1}$ and $\sim 1.49 \times 10^{-13} \text{ erg cm}^{-2} \text{ s}^{-1}$, respectively. These flux values correspond to $\sim 28\%$ and $\sim 34\%$ of the total observed flux in 2.0 - 10 keV band, respectively, and suggest that both the unabsorbed power law and the reflection components contribute substantially in this band.

Since Compton scattering is significant for large column densities and high energy photons (Yaqoob 1997), we applied the scattering component using **CABS** model to the primary transmitted component (model ‘M1 \ddagger ’ in Table 1). However, the **CABS** model does not account for the photons scattered into the line-of-sight from other directions. To account for this effect, we fitted the spectrum with a model (‘M1 \ddagger ’ in Table 1) in which the **PLCAB** model accounts for Compton scattering assuming a uniform, spherically distributed reprocessing material around the X-ray emitting source (Yaqoob 1997). This model also gives fit statistics ($\chi^2/\text{d.o.f.} \sim 32.5/27$) and parameters similar to the models ‘M1’ and ‘M1 \ddagger ’ (*cf.*, Table 1).

We also checked the spectral fitting with a model (‘M2’ in Table 1) in which the reflection component is accounted by the **REFLIONX** model (Ross & Fabian 2005). The **REFLIONX** model characterizes the reflected emission from an optically thick disc illuminated by radiation with a power law spectrum and produces the fluorescent emission lines as well as the continuum emission. The best-fit which could fit the Fe $K\alpha$ emission line gives unusually high Fe abundance (~ 10 times Solar), low ionization parameter ($\xi \sim 91_{-78}^{+160} \text{ erg cm s}^{-1}$) and photon index (Γ) of ~ 1.6 with $\chi^2/\text{d.o.f.} \sim 37.6/28$. The required high abundance and the low ionization parameter suggest that the Fe line emission is originating mainly from neutral or mildly ionized material.

Since the **PLCAB** model is valid up to energies between 10 and 18.5 keV and for column densities up to $\sim 5 \times 10^{24} \text{ cm}^{-2}$ (Yaqoob 1997), we attempted to use the **MYTORUS** model (Murphy & Yaqoob 2009) that accounts for the photoelectric absorption, Compton down-scattering as well as Fe $K\alpha$, $K\beta$ line emission and is valid for the 0.5 - 500 keV energy band and for column density up to 10^{25} cm^{-2} . This model considers an azimuthally symmetric toroidal geometry around AGN for the X-ray reprocessor and produces the reprocessed continuum and Fe $K\alpha$, Fe $K\beta$ lines self-consistently. The opening angle of the torus is fixed to 60° and the column density as well as the viewing angle are free parameters. The best-fit using the **MYTORUS** model (‘M5’) renders $N_{\text{H}} \sim 2.7 \times 10^{24} \text{ cm}^{-2}$, $\Gamma \sim 1.96$, and the viewing angle of the torus $\sim 90^\circ$, with $\chi^2/\text{d.o.f.} \sim 45/27$. The best-fit is obtained by fixing the viewing angle to 90° . If we allow it to vary, the fit statistics does not improve (*i.e.*, similar χ^2 value with decrease of 1 in d.o.f.) and gives viewing angle $\geq 88^\circ$ at 90% confidence level. We note that while using the **MYTORUS** model (‘M5’), an additional unabsorbed power law of photon index ~ 2.0 is required to fit the data below 10 keV.

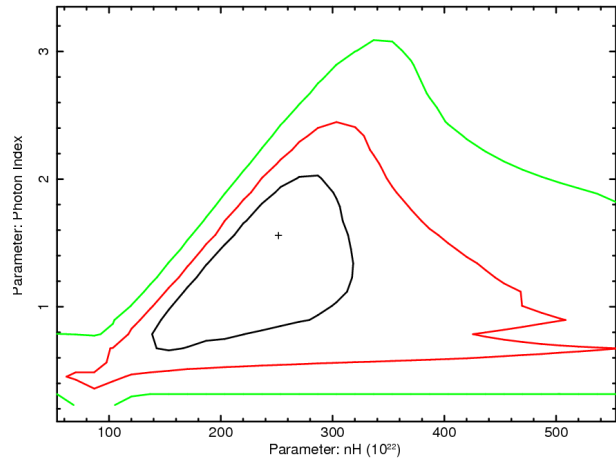


Figure 2. Confidence contours for the photon index versus absorbing column density obtained from model ‘M3’. Contours at 1σ , 2σ , and 3σ level are shown in Black, Red and Green, respectively.

We finally fitted the whole 0.5 - 50 keV spectrum with the above models and noted that addition of a thermal plasma model (**MEKAL** in XSPEC) of temperature $kT \sim 0.70 \text{ keV}$, is required to account for the emission below 2.0 keV (models ‘M3’, ‘M3 \ddagger ’, ‘M3 \ddagger ’ and ‘M4’ in Table 1). While fitting the 0.5 - 50 keV spectrum, we have excluded the XISs data points lying in 1.6 - 1.9 keV energy range because they are likely to be affected by systematic calibration uncertainties around the instrumental silicon K-edge. We find that the best-fit parameters obtained are similar in both the 2.0 - 50 keV and 0.5 - 50 keV spectral fittings. This implies that the addition or removal of the soft component ($E < 2.0 \text{ keV}$) does not affect the interpretation of the hard components. Table 1 lists the models and their resulting best-fit parameters. All the quoted errors are at 90% confidence level for one interesting parameter. The best-fitted spectrum using model ‘M3’ and the unfolded model are shown in Figure 1. Figure 2 shows the confidence contours for the photon index versus absorbing column density using model ‘M3’.

4 DISCUSSION

4.1 Soft X-ray emission

In our *Suzaku* X-ray spectral fitting, the soft X-ray emission below 2.0 keV is accounted by a thermal plasma model of temperature $kT \sim 0.70 \text{ keV}$ and a steep unabsorbed power law. The observed 0.5 - 2.0 keV luminosity is $\sim 1.66 \times 10^{41} \text{ erg s}^{-1}$ (*cf.*, Table 2), consistent with previous *ASCA* and *Chandra* observations within the measurement uncertainties. The ratio of soft X-ray to far infrared emission ($L_{0.5-2.0 \text{ keV}}/L_{\text{FIR}} \sim 3.0 \times 10^{-4}$ for NGC 5135) is consistent with the typical ratio observed in starburst galaxies (*e.g.*, Ranalli et al. (2003)), suggesting that the soft X-ray emission is dominated by starburst emission. Indeed, *Chandra* observation of high spatial resolution shows that the 0.5 - 2.0 keV soft X-ray emission from the central region is dominated by the circumnuclear starburst. The soft X-ray spectral components *i.e.*, thermal

Table 1. The best-fit spectral parameters

Energy range	Model	Soft Component		Hard Component			Fe K α line		χ^2/dof
		kT (keV)	Γ_{soft}	N_H ($\times 10^{24} \text{ cm}^{-2}$)	Γ_{hard}	R	E_{line} (keV)	EW_{Fe} (keV)	
2.0 - 50.0	M5	...	$2.04^{+0.26}_{-0.08}$	$2.71^{+0.81}_{-0.75}$	$1.96^{+0.26}_{-0.08}$	44.9/27
2.0 - 50.0	M1	...	$2.76^{+0.29}_{-0.25}$	$2.50^{+1.28}_{-0.92}$	$1.50^{+1.05}_{-0.71}$	$0.40^{+0.58}_{-0.27}$	$6.38^{+0.01}_{-0.01}$	$2.01^{+0.44}_{-0.27}$	32.8/28
2.0 - 50.0	M1 \dagger	...	$2.76^{+0.22}_{-0.18}$	$2.51^{+1.06}_{-1.08}$	$1.51^{+1.01}_{-0.66}$...	$6.38^{+0.01}_{-0.01}$	$2.14^{+0.36}_{-0.38}$	32.6/28
2.0 - 50.0	M1 \ddagger	...	$2.88^{+0.16}_{-0.22}$	$2.33^{+1.03}_{-0.91}$	$1.68^{+0.90}_{-0.71}$...	$6.38^{+0.01}_{-0.01}$	$2.09^{+0.42}_{-0.38}$	32.5/27
2.0 - 50.0	M2	...	$2.17^{+0.78}_{-0.52}$	$2.34^{+0.56}_{-0.36}$	$1.64^{+0.28}_{-0.16}$	37.6/28
0.5 - 50.0	M3	$0.67^{+0.09}_{-0.04}$	$2.73^{+0.19}_{-0.17}$	$2.59^{+1.04}_{-0.68}$	$1.55^{+1.09}_{-0.66}$	$0.42^{+1.64}_{-0.21}$	$6.38^{+0.01}_{-0.01}$	$2.10^{+0.46}_{-0.32}$	89.0/70
0.5 - 50.0	M3 \dagger	$0.73^{+0.07}_{-0.03}$	$2.82^{+0.18}_{-0.18}$	$2.74^{+1.76}_{-1.05}$	$1.59^{+1.02}_{-0.69}$...	$6.38^{+0.01}_{-0.01}$	$2.07^{+0.44}_{-0.38}$	91.4/70
0.5 - 50.0	M3 \ddagger	$0.67^{+0.08}_{-0.03}$	$2.71^{+0.19}_{-0.18}$	$2.30^{+1.00}_{-0.98}$	$1.60^{+0.97}_{-0.79}$...	$6.38^{+0.01}_{-0.01}$	$2.09^{+0.40}_{-0.28}$	89.0/70
0.5 - 50.0	M4	$0.80^{+0.06}_{-0.06}$	$2.31^{+0.12}_{-0.07}$	$2.20^{+0.36}_{-0.27}$	$1.65^{+0.26}_{-0.12}$	107.7/72

Notes:- M1: const(pl+wabs*pl+pexrav+line), M1 \dagger : const(pl+wabs*cabs*pl+pexrav+line),
M1 \ddagger : const(pl+plcabs+pexrav+line), M2: const(pl+wabs*pl+reffionx.mod),
M3: const(mekal+pl+wabs*pl+pexrav+line), M3 \dagger : const(mekal+pl+wabs*cabs*pl+pexrav+line),
M3 \ddagger : const(mekal+pl+plcabs+pexrav+line), M4: const(mekal+pl+wabs*pl+reffionx.mod), M5: MYTORUS
(Murphy & Yaqoob 2009).

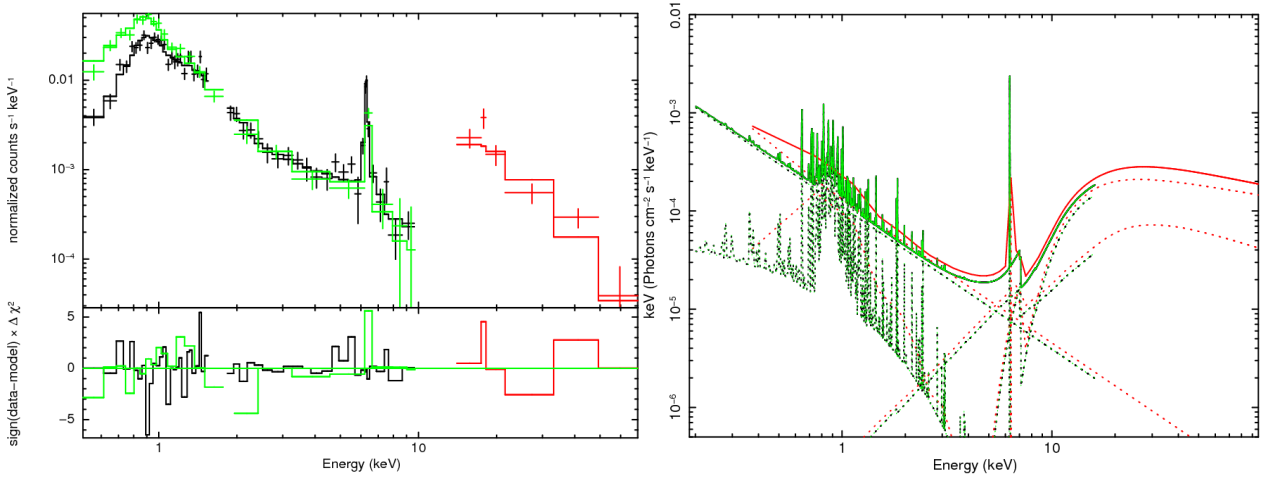


Figure 1. *Suzaku* 0.5 - 50 keV spectral fit using model ‘M3’. The left panel shows the spectral fit and residuals (in the bottom panel) and the right panel shows the unfolded model ‘M3’. The XIS0+3, XIS1 and HXD-PIN data points and spectral components are shown in Black, Green and Red, respectively. In unfolded model, the additive components are shown by dotted curves and cumulative model is shown by solid curves.

component of temperature $kT \sim 0.70$ keV and a steep power law ($\Gamma \sim 2.7$), in our *Suzaku* data are fairly consistent with the X-ray spectral properties of a spatially-resolved strong circumnuclear starburst region identified in *Chandra* observation (Levenson et al. 2004). The steep unabsorbed power law is likely to have contribution from different individual sources, mainly X-ray binaries in the starburst region (Zezas et al. 2002). High resolution near-IR study of the central ~ 2.3 kpc region in NGC 5135 has revealed the star formation knots and a large ~ 600 pc [Si VI] $1.96\mu\text{m}$ line emission ionization cone centered on AGN (Bedregal et al. 2009). It has been argued that SNR shocks play a dominant role in ionizing the gas in central ~ 2.3 kpc region and photoionized emission due to AGN as well as the recent star formation have rather localized and smaller contribution (Bedregal et al. 2009). We note the fact that in general, high resolution X-ray grating spectral studies show that the soft X-ray emission in Seyfert 2s

is dominated by recombination lines implying photoionization as the primary mechanism (Kinkhabwala et al. 2002; Guainazzi & Bianchi 2007; Marinucci et al. 2011). However, the soft X-ray emission in Seyfert 2s with intense circumnuclear starburst, is likely to be dominated by collisionally ionized optically thin plasma emission associated with star formation (Guainazzi et al. 2009). Limited spatial and spectral resolution of the *Suzaku* XIS CCD does not allow us to quantify the AGN and starburst contribution to the 0.5 - 2.0 keV soft X-ray emission, which in turn, unable us to draw firm conclusions about the origin of the soft X-ray emission. X-ray observations of high spectral and spatial resolution are required to confirm the nature of the soft X-ray emission in NGC 5135.

Table 2. *Suzaku* X-ray fluxes and luminosities of NGC 5135

Energy (keV)	Model	F_{obs} ($\text{erg cm}^{-2} \text{ s}^{-1}$)	L_{obs} (erg s^{-1})	$\frac{F_{\text{cor}}}{F_{\text{obs}}}$
0.5 - 2.0	M3	3.89×10^{-13}	1.66×10^{41}	5.0
	M3 [†]	3.89×10^{-13}	1.66×10^{41}	65.9
	M3 [‡]	3.89×10^{-13}	1.66×10^{41}	16.6
	M4	3.88×10^{-13}	1.66×10^{41}	12.3
2.0 - 10	M3	4.44×10^{-13}	1.89×10^{41}	11.3
	M3 [†]	4.40×10^{-13}	1.87×10^{41}	124.8
	M3 [‡]	4.43×10^{-13}	1.89×10^{41}	27.0
	M4	4.37×10^{-13}	1.86×10^{41}	20.5
10 - 50	M5	4.17×10^{-13}	1.78×10^{41}	135.5
	M3	1.58×10^{-11}	6.67×10^{42}	1.2
	M3 [†]	1.50×10^{-11}	6.39×10^{42}	8.4
	M3 [‡]	1.50×10^{-11}	6.67×10^{42}	1.7
	M4	1.49×10^{-11}	6.35×10^{42}	1.3
Fe K α	M5	1.46×10^{-11}	6.17×10^{42}	4.5
	M3	9.35×10^{-14}	3.98×10^{40}	...

Notes:- F_{obs} : observed flux, L_{obs} : observed luminosity, F_{cor} : absorption corrected flux.

4.2 Hard X-ray emission

Our *Suzaku* X-ray spectral fitting shows that the 2.0 - 10 keV continuum emission has contribution from several spectral components *e.g.*, steep unabsorbed power law, thermal plasma model, reflection component, absorbed power law (see, Figure 1). However, the relative contribution from each individual spectral component is energy dependent. For example, the relative contribution of the unabsorbed power law decreases towards higher energies, while it increases for the reflection component. The thermal plasma model and absorbed power law components contribute only to the soft and hard part of the 2.0 - 10 keV band, respectively. Using SFR - X-ray correlation ($\text{SFR} \simeq 2.0 \times L_{2.0-10 \text{ keV}} M_{\odot} \text{ yr}^{-1}$) from Ranalli et al. (2003) and assuming $\text{SFR} \sim 15 M_{\odot} \text{ yr}^{-1}$ in NGC 5135 (Bedregal et al. 2009), we noted that the estimated contribution from the circumnuclear starburst to the 2.0 - 10 keV X-ray luminosity is $\sim 7.5 \times 10^{40} \text{ erg s}^{-1}$, which $\sim 40\%$ of the total observed 2.0 - 10 keV luminosity. This value is similar to the 2.0 - 10 keV non-AGN X-ray luminosity reported in *Chandra* observation, which could spatially resolve the AGN and circumnuclear starburst X-ray emission (Levenson et al. 2004). Above argument infers that nearly $\sim 60\%$ of the total observed 2.0 - 10 keV X-ray emission is attributed to AGN emission, which is accounted by the scattered, reflected and transmitted components. Our *Suzaku* (0.5 - 50 keV) broad-band X-ray spectral analysis of NGC 5135 shows the characteristics of starburst as well as obscured AGN and thus confirming its composite nature. Furthermore, the X-ray emission from circumnuclear starburst regions in NGC 5135 can be characterized by both thermal plasma model plus unabsorbed power law (Levenson et al. 2004). It is noted that star-forming galaxies show characteristic power law X-ray emission that could be the integrated spectrum of distinct X-ray sources (Zezas et al. 2002). Moreover, an unabsorbed power law component representing the scattered emission of the primary AGN continuum to the line-of-sight is also commonly seen in obscured AGNs (Braitto et al. 2009; Comastri et al. 2010; Severgnini et al. 2011). With present

Suzaku data we cannot spatially separate out the AGN and circumnuclear starburst emission and therefore it is possible that the unabsorbed power law component in our spectral fitting may have contribution from both the **circumnuclear** starburst as well as the scattered component of AGN emission. It is likely that the quality of the present 2.0 - 50 keV *Suzaku* data do not allow us to accurately determine the relative contributions from starburst, scattered, reflected and absorbed AGN emission spectral components in the 2.0 - 10 keV energy band.

Our *Suzaku* 2.0 - 50 keV broad-band spectral fitting clearly shows that the hard X-ray continuum is characterized by a heavily absorbed power law and a reflection component, consistent with the previous results reported by Fukazawa et al. (2011). The high absorbing column density ($N_{\text{H}} \sim 2.5 \times 10^{24} \text{ cm}^{-2}$) and the high ratio of the intrinsic to the observed 2.0 - 10 keV flux/luminosity (see, Table 2) infer the presence of a heavily obscured, luminous AGN. The ratio of the intrinsic to the observed flux/luminosity in 2.0 - 10 keV band, found for NGC 5135, is consistent with the typical values observed in other Compton-thick AGNs (Levenson et al. 2006; Brightman & Nandra 2011). Given the importance of Compton scattering in absorbers with column densities of a few times of 10^{24} cm^{-2} , the absorption corrected (intrinsic) flux/luminosity is model-dependent. The value of the intrinsic luminosity ($\frac{L_{2.0-10 \text{ keV, int}}}{L_{2.0-10 \text{ keV, obs}}} \sim 125$) obtained from the model ‘M3[†]’ which uses the CABS model for the scattering, can be considered as the upper limit. Since the CABS model represents the Compton scattering from the matter only along the line-of-sight and therefore offers a small covering fraction *i.e.*, a single cloud along the line-of-sight which only removes photons from the beam owing to Compton scattering and does not consider the addition of photons scattered from other directions into the line-of-sight. Moreover, the ratio of the intrinsic to the observed flux/luminosity also depends on the photon index of the intrinsic power law, for example, this ratio obtained from M3[†] model is as high as ~ 300 , if we fix the photon index to 1.9. The value of the intrinsic luminosity obtained from the model ‘M3[‡]’ where the PLCABS model is used for scattering can be considered as a lower limit, since in this scenario, the contribution from photons initially not in the line-of-sight, which are then scattered to the line-of-sight, is highest, and roughly compensate the loss of photons which are initially along the line-of-sight, and that are scattered out. Thus, the two models represent two limits: a single cloud covering (CABS) gives an upper limit and full covering (PLCABS) gives a lower limit on the intrinsic luminosity, and the true value lies somewhere in between depending on the covering factor. In the MYTORUS model covering factor corresponds to 0.5 and the ratio of the intrinsic to the observed flux/luminosity (~ 135) indeed lies between the two limits, if the photon index of the intrinsic power law is assumed to be 1.9.

High obscuration around the AGN is also inferred from the flux ratio of hard (2.0 - 10 keV) X-ray to [OIII] $\lambda 5007\text{\AA}$ line emission (Bassani et al. 1999), *i.e.*, for NGC 5135, we obtain $\log[F_{2.0-10 \text{ keV, obs}}/F_{[\text{OIII}]}] \simeq -1.1$, using the reddening-corrected [OIII] flux given in Singh et al. (2011). Furthermore, the flux ratio of the intrinsic 2.0 - 10 keV hard X-ray to [OIII] $\lambda 5007\text{\AA}$ line emission is ($F_{2.0-10 \text{ keV, int}}/F_{[\text{OIII}]}$) ~ 9.2 , consistent with the mean ratio of observed in Seyfert

1 galaxies (Heckman et al. 2005), supporting the notion that the obscured nucleus in NGC 5135 is intrinsically similar to a Seyfert type 1 nuclei.

Signature of Compton-thick matter around the AGN can be characterized by Compton reflection continuum with a broad hump peaking around 20 - 30 keV, which rapidly decreases at both low and high energies due to photoelectric absorption and Compton down-scattering, respectively. In our spectral fits the reflection strength measured as the ratio of the normalizations of the reflection component to the transmitted component (absorbed power law) is ~ 0.4 (using model ‘M1’). We do not attempt to compare the strengths of the reflection components obtained by using the MYTORUS model and the PEXRAV model since these models consider different geometries for the reprocessor. The relative strength of the reflection continuum very critically depends on geometry since it is affected by the angle of reflection integrated over the surface of the reprocessor. Murphy & Yaqoob (2009) showed that the reflection spectrum from a Compton-thick face-on torus that subtends the same solid angle as a Compton-thick face-on accretion disc at the X-ray source is much weaker and it is not meaningful to compare the reflection strength given by the MYTORUS model with one from the PEXRAV model.

4.3 Geometry of the absorber

It is important to note that the PEXRAV as well as REFLIONX models consider reflection from the surface of accretion disc and therefore, are insufficient to constrain the geometry of the toroidal-shaped obscuring material around the AGN. We used the MYTORUS model (Murphy & Yaqoob 2009) that considers the geometry of reprocessing material as an azimuthally symmetric obscuring torus. This model suggests the edge-on view (*i.e.*, the viewing angle $\sim 90^\circ$) of the obscuring torus. The absorbing column density given by the MYTORUS model corresponds to the equatorial column density of the toroidal-shaped obscuring material. We note that the column densities obtained from the MYTORUS and other models are similar within the uncertainties (see, Table 1) and therefore, it again confirms that the obscuring torus is oriented nearly edge-on. We caution that in the current version of the MYTORUS model, the torus opening angle is fixed to 60° while it **needs** to be a varying parameter. The opening angle of 60° corresponds to covering factor of 0.5 and the solid angle subtended by the torus on to the X-ray emitting source to 2π . Hints on the covering fraction of the absorber, as seen from the X-ray source, can be inferred from our fits. It has been shown that variation in the geometry of obscuring torus, and not the iron abundance or intrinsic spectral shape, is required to produce EWs significantly larger than 1 keV and therefore, EW of Fe $K\alpha$ line can be used to place limits on the covering factor (Levenson et al. 2002). Levenson et al. (2002) argued that the high EW of Fe $K\alpha$ line (~ 2.1 keV) in NGC 5135 suggests a small opening angle ($\sim 20^\circ$) of the obscuring torus giving a covering fraction of $\sim 90\%$. Our *Suzaku* X-ray spectral fitting gives $L_{\text{Fe}} \simeq 3.98 \times 10^{40}$ erg s $^{-1}$ and using Levenson et al. (2006) empirical ratio of Fe $K\alpha$ line luminosity to intrinsic 2.0 - 10 keV luminosity we obtain $L_{2-10 \text{ keV, int}} \sim 1.99 \times 10^{43}$ erg s $^{-1}$, *i.e.*, nearly 100 times the observed 2.0 - 10.0 keV luminosity. This value of the 2.0 - 10 keV intrinsic luminosity lies between the val-

ues from the MYTORUS model (covering fraction $\sim 50\%$) and the M3 ‡ model that uses the PLCABS model (covering fraction $\sim 100\%$). Furthermore, we note that the intrinsic 2.0 - 10 keV X-ray luminosity obtained by using the mid-IR (12 μm) - X-ray luminosity correlation ($L_{\text{MIR}} - L_{2.0-10 \text{ keV}}$) and mid-IR luminosity ($L_{\text{MIR}} \sim 1.15 \times 10^{43}$ erg s $^{-1}$) given in Gandhi et al. (2009), is $\sim 7.6 \times 10^{42}$ erg s $^{-1}$, that again lies between than the values from the model M5 and M3 ‡ . The high resolution mid-IR core fluxes/luminosities presented in Gandhi et al. (2009) are reported to be least contaminated by the circumnuclear starburst and primarily represent the emission from the torus. The above comparisons for the 2.0 - 10 keV intrinsic luminosities suggest that the covering factor lies between 50% to 100%. Finally, the low ratio between the soft power law flux and the intrinsic emission (< 0.01 , Table 2) suggests a low scattering efficiency, which again, may be due to a high covering factor of the thick absorber, leaving only a small fraction of the solid angle free for the primary continuum to reach the warm scatterer. A similar low flux ratio (< 0.01) of the unabsorbed powerlaw to the intrinsic 2.0 - 10 keV emission is obtained with the model ‘M5’ which considers an axi-symmetric toroidal geometry of the reprocessing material around the AGN. The actual scattered fraction may be even lower, given that part of the soft power law may be due to the starburst emission.

5 CONCLUSIONS

We analyzed the *Suzaku* XIS + HXD-PIN observation of the AGN in NGC 5135. We found that the 0.5 - 50 keV spectrum can be reproduced by a model consisting of: (i) a soft component, characterized by a thermal plasma model (the MEKAL) of temperature $kT \sim 0.70$ keV plus an unabsorbed steep power law ($\Gamma \sim 2.7$), (ii) a hard component best fitted by an absorbed power law ($N_{\text{H}} \sim 2.5 \times 10^{24}$ cm $^{-2}$, $\Gamma \sim 1.6$), a reflection continuum component and a prominent Fe $K\alpha$ line with EW ~ 2.1 keV. *Suzaku* broad-band energy coverage allowed us to accurately measure the absorbing column density, intrinsic AGN luminosity and the reflection component. We attempted various physically motivated models and all the models confirm that the AGN in NGC 5135 is obscured by Compton-thick material. The MYTORUS model which considers the geometry of the reprocessing material as a azimuthally symmetric torus suggests that the torus is viewed nearly edge on. Both the estimates on the reflection strength and the comparison between the emission line flux and the continuum flux suggest that the obscuring torus may cover 90% of the line-of-sight. Our *Suzaku* X-ray spectral study of NGC 5135 may represent a case study of some of the complex features in Compton-thick obscured AGNs.

ACKNOWLEDGMENTS

This research has made use of data obtained from the *Suzaku* satellite, a collaborative mission between the space agencies of Japan (JAXA) and the USA (NASA). Authors also thank to the anonymous referee for useful comments that helped to improve the quality of the paper.

REFERENCES

- Antonucci R., 1993, *ARAA*, 31, 473
 Bassani L., et al., 1999, *ApJS*, 121, 473
 Beckmann V., et al., 2009, *A&A*, 505, 417
 Bedregal A. G., Colina L., Alonso-Herrero A., Arribas S., 2009, *ApJ*, 698, 1852
 Braitto V., Reeves J. N., Della Ceca R., Ptak A., Risaliti G., Yaqoob T., 2009, *A&A*, 504, 53
 Brightman M., Nandra K., 2011, *MNRAS*, 413, 1206
 Cappi M., et al., 2006, *A&A*, 446, 459
 Comastri A., Iwasawa K., Gilli R., Vignali C., Ranalli P., Matt G., Fiore F., 2010, *ApJ*, 717, 787
 Della Ceca R., et al., 2008, *MmSAI*, 79, 65
 Fukazawa Y., et al., 2009, *PASJ*, 61, 17
 Fukazawa Y., et al., 2011, *ApJ*, 727, 19
 Gandhi P., et al., 2009, *A&A*, 502, 457
 González Delgado R. M., et al., 1998, *ApJ*, 505, 174
 Guainazzi M., et al., 2009, *A&A*, 505, 589
 Guainazzi M., Bianchi S., 2007, *MNRAS*, 374, 1290
 Hasinger G., 2008, *A&A*, 490, 905
 Heckman T. M., Ptak A., Hornschemeier A., Kauffmann G., 2005, *ApJ*, 634, 161
 Kinkhabwala A., et al., 2002, *ApJ*, 575, 732
 Koyama K., et al., 2007, *PASJ*, 59, 23
 Levenson N. A., et al., 2002, *ApJL*, 573, L81
 Levenson N. A., Heckman T. M., Krolik J. H., Weaver K. A., Życki P. T., 2006, *ApJ*, 648, 111
 Levenson N. A., Weaver K. A., Heckman T. M., Awaki H., Terashima Y., 2004, *ApJ*, 602, 135
 Magdziarz P., Zdziarski A. A., 1995, *MNRAS*, 273, 837
 Maiolino R., et al., 1998, *A&A*, 338, 781
 Marinucci A., et al., 2011, *A&A*, 526, A36+
 Matt G., Fabian A. C., Guainazzi M., Iwasawa K., Bassani L., Malaguti G., 2000, *MNRAS*, 318, 173
 Mitsuda K., et al. 2007, *PASJ*, 59, 1
 Murphy K. D., Yaqoob T., 2009, *MNRAS*, 397, 1549
 Nandra K., Pounds K. A., 1994, *MNRAS*, 268, 405
 Phillips M. M., Charles P. A., Baldwin J. A., 1983, *ApJ*, 266, 485
 Ranalli P., Comastri A., Setti G., 2003, *A&A*, 399, 39
 Risaliti G., Maiolino R., Salvati M., 1999, *ApJ*, 522, 157
 Ross R. R., Fabian A. C., 2005, *MNRAS*, 358, 211
 Serlemitsos P. J., et al., 2007, *PASJ*, 59, 9
 Severgnini P., et al., 2011, *A&A*, 525, A38+
 Singh V., Shastri P., Risaliti G., 2011, *A&A*, 532, A84+
 Takahashi T., et al., 2007, *PASJ*, 59, 35
 Tueller J., et al., 2008, *ApJ*, 681, 113
 Turner T. J., George I. M., Nandra K., Mushotzky R. F., 1997, *ApJS*, 113, 23
 Yaqoob T., 1997, *ApJ*, 479, 184
 Zezas A., Fabbiano G., Rots A. H., Murray S. S., 2002, *ApJ*, 577, 710